1 Hamiltonian systems

A Hamiltonian system is described by

$$\begin{matrix} & \mathcal{H}(p_1,\dots p_N,q_1,\dots q_N) & \\ \dot{q}_i = \dfrac{\partial \mathcal{H}}{\partial p_i} & & \dot{p}_i = -\dfrac{\partial \mathcal{H}}{\partial q_i} \end{matrix} \tag{1}$$

where the q_i are considered to be positions and p_i momenta. The convention in Hamiltonian systems is to define the **number of degrees of freedom** to be N. In contrast, in the convention used for dissipative systems, we would say that (1) has $2N$ degrees of freedom.

A Hamiltonian system conserves volumes in (p_i, q_i) space. Writing

$$\dot{\mathbf{x}} = \mathbf{f}(x) \tag{2}$$

we have

$$\begin{aligned} V(t+dt)-V(t) &= dt\int_{\text{surface}} \mathbf{f}\cdot\mathbf{n}\; da = dt\int_{\text{volume}} \nabla\cdot\mathbf{f} dv = dt\int_{\text{volume}} \sum_i \frac{\partial \dot{x}_i}{\partial x_i}\; dv \\ &= dt\int_{\text{volume}} \sum_i \left(\frac{\partial \dot{q}_i}{\partial q_i}+\frac{\partial \dot{p}_i}{\partial p_i}\right)\; dv = dt\int_{\text{volume}} \sum_i \left(\frac{\partial^2 \mathcal{H}}{\partial q_i \partial p_i}-\frac{\partial^2 \mathcal{H}}{\partial q_i \partial p_i}\right)\; dv = 0 \end{aligned} \tag{3}$$

Although Hamiltonian systems were originally developed in the eighteenth century to describe celestial mechanics, they are now used in many, if not most, fields of physics, such as plasma physics (for example, the fields in a Tokamak) and quantum systems (for example, quantum optics and Bose-Einstein condensation).

One realization of a Hamiltonian system that is very relevant to fluid mechanics is the streamfunction $\psi(x,y)$ describing two-dimensional velocity fields via $\mathbf{u} = \mathbf{e_z}\times\nabla\psi$. A particle at position (x,y) moves according to:

$$\frac{dx}{dt} = u = -\frac{\partial \psi}{\partial y} \qquad \frac{dy}{dt} = v = \frac{\partial \psi}{\partial x} \tag{4}$$

Particles move along streamlines, i.e. curves of constant ψ, just as trajectories move along curves/surfaces of constant energy $\mathcal{H}$ in the general formulation.

2 Integrable systems

A Hamiltonian system with N degrees of freedom is **integrable** if there exist N functions $F_j(\mathbf{p},\mathbf{q})$ such that

$$\frac{dF_j}{dt} = 0 \tag{5}$$

and

$$[F_j, F_k] \equiv \sum_i \left(\frac{\partial F_j}{\partial q_i}\frac{\partial F_k}{\partial p_i} - \frac{\partial F_j}{\partial p_i}\frac{\partial F_k}{\partial q_i}\right) = 0 \tag{6}$$

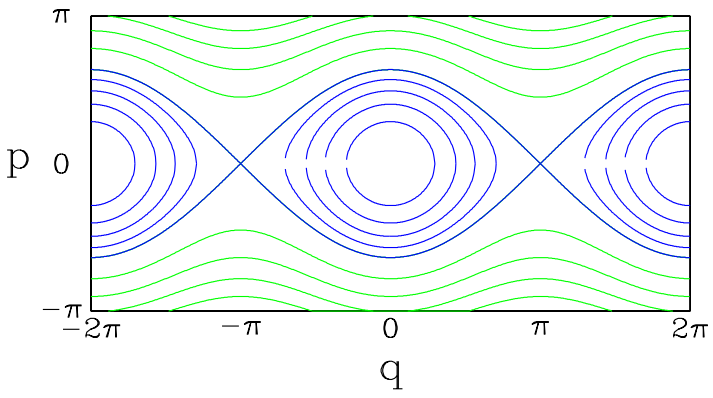

Figure 1: Phase portrait for the classic pendulum.

Note that $\mathcal{H}$ already provides one of the F_j, since

$$\frac{d\mathcal{H}}{dt} = \sum_i \left(\frac{\partial \mathcal{H}}{\partial q_i}\dot{q}_i + \frac{\partial \mathcal{H}}{\partial p_i}\dot{p}_i \right) = \sum_i \left(\frac{\partial \mathcal{H}}{\partial q_i}\frac{\partial \mathcal{H}}{\partial p_i} - \frac{\partial \mathcal{H}}{\partial p_i}\frac{\partial \mathcal{H}}{\partial q_i} \right) = 0 \tag{7}$$

In addition,

$$[F_j, \mathcal{H}] = \sum_i \left(\frac{\partial F_j}{\partial q_i}\frac{\partial \mathcal{H}}{\partial p_i} - \frac{\partial F_j}{\partial p_i}\frac{\partial \mathcal{H}}{\partial q_i} \right) = \sum_i \left(\frac{\partial F_j}{\partial q_i}\dot{q}_i + \frac{\partial F_j}{\partial p_i}\dot{p}_i \right) = \frac{dF_j}{dt} \tag{8}$$

so that $dF_j/dt = 0$ implies

$$[F_j, \mathcal{H}] = 0 \tag{9}$$

Thus any system with one degree of freedom is integrable, and $N-1$ functions F_j satisfying (5) and (6) are necessary in order for an N-degree-of-freedom system to be integrable.

For an integrable system, there exists a transformation

$$\begin{aligned} (\mathbf{I}, \theta) &\leftarrow (\mathbf{p}, \mathbf{q}) \\ \mathcal{H}'(\mathbf{I}, \theta) &= \mathcal{H}(\mathbf{p}, \mathbf{q}) \end{aligned} \tag{10}$$

where, in fact,

$$\mathcal{H}'(\mathbf{I}, \theta) = \mathcal{H}'(\mathbf{I}) \tag{11}$$

so that the dynamics in the $(\mathbf{I}, \theta)$ variables are

$$\begin{aligned} \dot{I}_i &= -\frac{\partial \mathcal{H}'}{\partial \theta_i} = 0 & \qquad \dot{\theta}_i &= \frac{\partial \mathcal{H}'}{\partial I_i} = \omega_i(\mathbf{I}) \\ I_i(t) &= I_i(0) & \qquad \theta(t) &= \theta(0) + t\omega_i \end{aligned} \tag{12}$$

The flow (12) is called a **twist map** and $(\mathbf{I}, \theta)$ are called the **action-angle** variables.

We illustrate the transformation to action-angle variables for the classic pendulum, whose Hamiltonian is given by

$$\mathcal{H} = \frac{1}{2}p^2 - \cos q \tag{13}$$

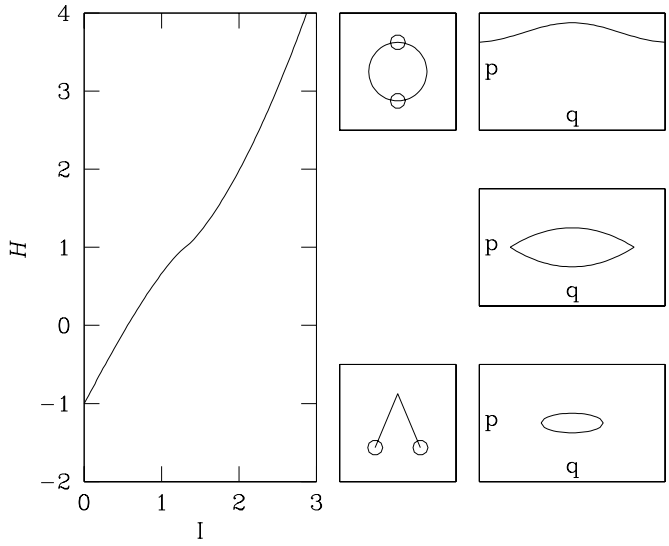

Figure 2: Left: Function $\mathcal{H}$ which describes the pendulum in terms of the canonical action variable I. Middle: pendulum configuration for $\mathcal{H} > 1$ consists of repeated clockwise or counterclockwise rotations, while that for $\mathcal{H} < 1$ corresponds to small oscillations. Right: corresponding trajectories in the (q, p) plane, including limiting heteroclinic orbit at $\mathcal{H} = 1$ with $\omega = d\mathcal{H}/dI = 0$.

and whose phase portrait is shown in figure 1. We take $m = g = 1$ and do not distinguish between momentum and velocity. We use q to denote the angle and p the velocity/momentum, reserving the usual θ for the "angle" of the action-angle transformation.

$$I \equiv \frac{1}{2\pi} \oint p dq \tag{14}$$

The integral is taken over a closed trajectory, on which $\mathcal{H}$ has the constant value H. For the pendulum, we write

$$\begin{aligned} H &= \frac{1}{2}p^2 - \cos q \\ p^2 &= 2(H + \cos q) \\ p &= \sqrt{2(H + \cos q)} \\ I &= \frac{1}{2\pi} \int_0^{2\pi} \sqrt{2(H + \cos q)}\, dq \end{aligned} \tag{15}$$

Equation (15) gives I as a function of the value of H, and can, in principle, be inverted to define $\mathcal{H}'$ as a function of I. A new angle is also defined whose rate of change is constant in time. Figure 2 shows the function $\mathcal{H}'(I)$, along with an interpretation in terms of the pendulum configurations and the original (q, p) phase space.

3 Non-integrable perturbation to an integrable system

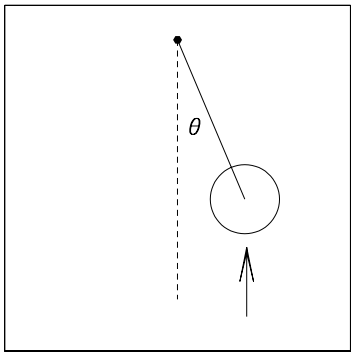

Figure 3: Kicked rotor. The rotor is in the horizontal plane and receives a "kick" with period τ.

Since all Hamitonian systems with one degree of freedom are integrable, the simplest systems we can examine for non-integrability are of the form:

$$\mathcal{H}(p_1, p_2, q_1, q_2) \qquad \text{a system with } N = 2 \text{ degrees of freedom} \tag{16}$$

or

$$\mathcal{H}(p, q, t) \qquad \text{sometimes called a system with } N = 1.5 \text{ degrees of freedom} \tag{17}$$

A simple system of type (17) is the kicked rotor, a pendulum which rotates in the horizontal plane (thus without the action of gravity) and which is given an impulsional acceleration in the same direction at times $t = 0, \tau, 2\tau, \ldots$, as illustrated in figure 3.

$$\begin{aligned} \mathcal{H}(v, \theta, t) &= \frac{v^2}{2} + \epsilon \cos\theta \sum_n \delta(t - n\tau) \\ \dot{\theta} = \frac{\partial \mathcal{H}}{\partial v} = v & \qquad \theta_{n+1} - \theta_n = v_n \bmod 2\pi \\ \dot{v} = -\frac{\partial \mathcal{H}}{\partial \theta} = \epsilon \sin\theta \sum_n \delta(t - n\tau) & \qquad v_{n+1} - v_n = \epsilon \sin\theta_{n+1} \end{aligned} \tag{18}$$

We write (18) as:

$$\mathcal{H} = \mathcal{H}_0(\theta, v) + \epsilon\, \mathcal{H}_1(\theta, v, t) \tag{19}$$

where

$$\mathcal{H}_0 = \frac{v^2}{2} \tag{20}$$

Not only is $\mathcal{H}_0 = v^2/2$ integrable, but it is already written in action-angle variables (so we have used $\theta \sim q$ and $p \sim v$). As is always the case for action-angle variables, the phase space consists of a set of concentric curves, each with its own (constant) angular velocity. For this simple case, $I \sim p \sim v \sim \omega \sim r$, and we will use all of these variables to denote the same quantity. The behavior of this simple flow is illustrated in figure 4. To simplify further, we will set $\tau = 2\pi$.

In order to prepare to consider the perturbed system (19), we define the Poincaré or first return map arising from $\mathcal{H}_0$:

$$T_0(I, \theta) = (I, \theta)(t = 2\pi) = (I, (\theta + 2\pi I) \bmod 2\pi) \tag{21}$$

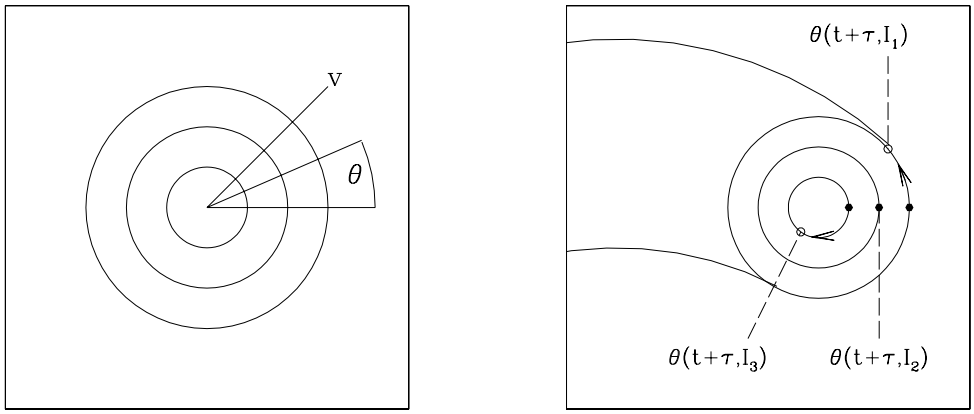

Figure 4: Behavior of unperturbed twist map. Left: Domain (I, θ) consists of concentric circles, each corresponding to one value of $I = v$. Flow on each circle is rotation with velocity v. Right: Solid circles are positions of three points $\theta(t, I_1), \theta(t, I_2), \theta(t, I_3)$. Hollow circles are positions at later time $t + \tau$. Value I_2 corresponds to $v = 0$. The domain can be extended to a torus, with the new angular direction corresponding to time.

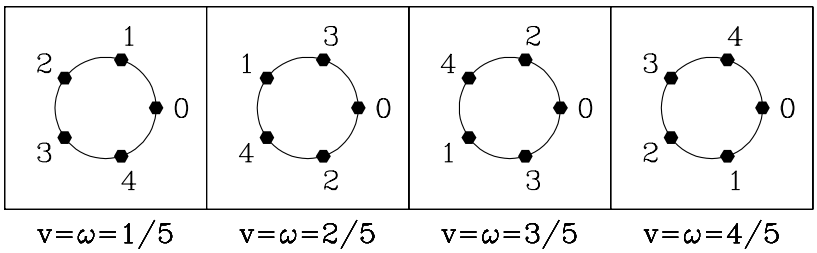

Figure 5: Five-cycles of map T_0 corresponding to multiples of 1/5.

where (I, θ) evolve according to the Hamiltonian $\mathcal{H}_0$ and, when the time is not specified, (I, θ) refers to their values at $t = 0$. Each circle is invariant under T_0, but its individual points are not necessarily invariant. The $v = 0$ circle consists of fixed points, but the $v = 1/2$ circle consists of 2-cycles, the $v = 1/3$ circle consists of 3-cycles and so on. Some five-cycles are shown in figure 5.

We also define the n^{th} iterate of T_0.

$$T_0^n(I, \theta) = (I, \theta)(t = 2\pi n) = (I, (\theta + 2\pi n\, I) \bmod 2\pi) \tag{22}$$

If $v = I = \omega(I) = m/n$, then

$$T_0^n(I, \theta) = \left(I, (\theta + 2\pi\, n\, \frac{m}{n}) \bmod 2\pi\right) = (I, (\theta + 2\pi\, m) \bmod 2\pi) = (I, \theta) \tag{23}$$

so the circles $I = m/n$ consist of fixed points of T_0^n.

4 Poincaré-Birkhoff Theorem

We now re-introduce the perturbation:

$$\mathcal{H}_\epsilon \equiv \mathcal{H}_0 + \epsilon\,\mathcal{H}_1 \tag{24}$$

and the corresponding maps

$$T_\epsilon^n(I,\theta) \equiv (I,\theta)(t = 2\pi\, n) \tag{25}$$

where I and θ now evolve according to the Hamiltonian $\mathcal{H}_\epsilon$.

The **Poincaré-Birkhoff theorem** concerning the map T_ϵ^n acting on the curve $I = m/n$ states:
–The image of (I,θ) under T_ϵ^n is

$$T_\epsilon^n(I,\theta) = (I',\theta)$$

That is, under the mapping T_ϵ^n, the radius changes, but not the angle.
–The curves (I,θ) and (I',θ) intersect each other a multiple of $2n$ times, creating a set of alternating hyperbolic and elliptic points.
–The area inside (I',θ) is the same as that inside (I,θ).

The Poincaré-Birkhoff theorem is illustrated in figures 6 and 7. Note that each of the new elliptic points is now surrounded by invariant circles, some of which have rational winding numbers. The Poincaré-Birkhoff theorem applies recursively to each of them!

So far we have discussed the fate of the elliptic points and the orbits surrounding them. What happens to hyperbolic points, in particular the new hyperbolic points mentioned by the Poincaré-Birkhoff theorem and illustrated in the right portion of figure 7?

For integrable Hamiltonian systems, heteroclinic and homoclinic connections are typical. However, for non-integrable Hamiltonian systems, they are not. Define the **unstable manifold** and **stable manifold** of the hyperbolic points A and B as the points which approach A or B in iterating backwards or forwards:

$$W^U(A) \equiv \left\{ x : \lim_{k\to\infty} T^{-k}(x) = A \right\} \tag{26a}$$

$$W^S(B) \equiv \left\{ x : \lim_{k\to\infty} T^{k}(x) = B \right\} \tag{26b}$$

In the heteroclinic situation illustrated in the left portion of figure 8, $W^U(A)$ and $W^S(B)$ are identical, as can occur for an integrable Hamiltonian system. The right portion of figure 8 shows that when a non-integrable perturbation is introduced, these two manifold cross transversely, at a point C. Under further iteration forwards and backwards in time, C is mapped into other points, all belonging to the intersection of $W^U(A)$ and $W^S(B)$. Since A and B are attained only after an infinite number of iterations, an infinite number of such intersections of $W^U(A)$ and $W^S(B)$ exist, accumulating at A and B. Since areas are conserved and the intersections take place along decreasing distances, the perpendicular directions increase, creating a pair of **homoclinic tangles** near A and B. A single homoclinic tangle is illustrated in figure 9. A homoclinic tangle implies **chaos**, that is, the separation of nearby points under iteration, also called **sensitivity to initial conditions**.

The combined complexity of the chains of elliptic and hyperbolic points and the homoclinic tangles was said by Poincaré to be too complicated to describe. An effort to depict it nonetheless is given in figure 10.

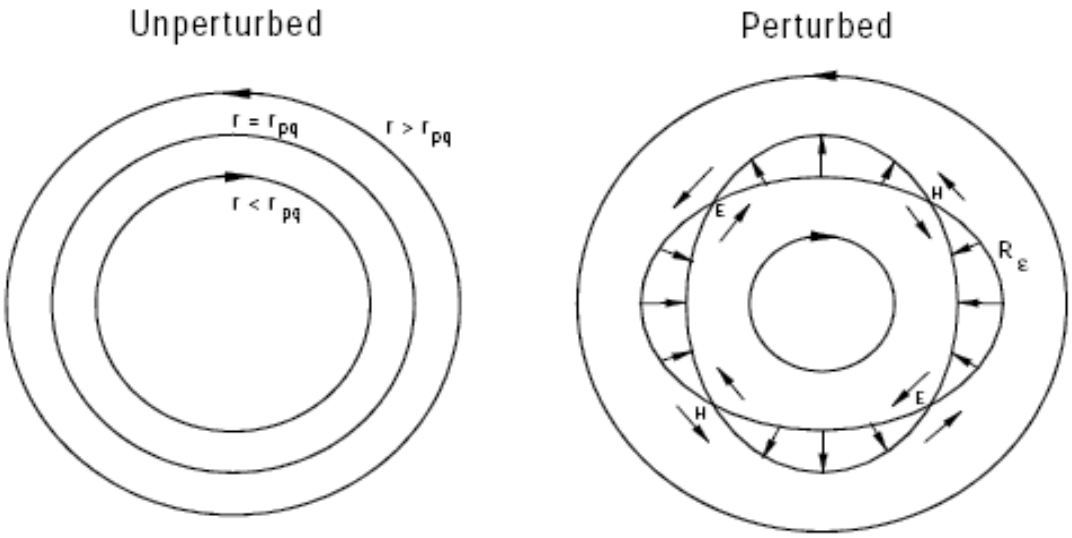

Figure 6: Dynamics of T^n near a circle for which $I = m/n$ (written as r_{pq} in the figure). Left: unperturbed system. Points on intermediate circle are fixed, while those on outer (inner) circle rotate counterclockwise (clockwise). Right: perturbed system. According to the Poincaré-Birkhoff theorem, curves (I, θ) and $T^n_\epsilon(I, \theta) = (I', \theta)$ intersect an even number of times at an alternating set of elliptic and hyperbolic fixed points. This can be seen by considering the angular flow (counterclockwise outside and clockwise inside) and the radial flow (alternating inwards and outwards).

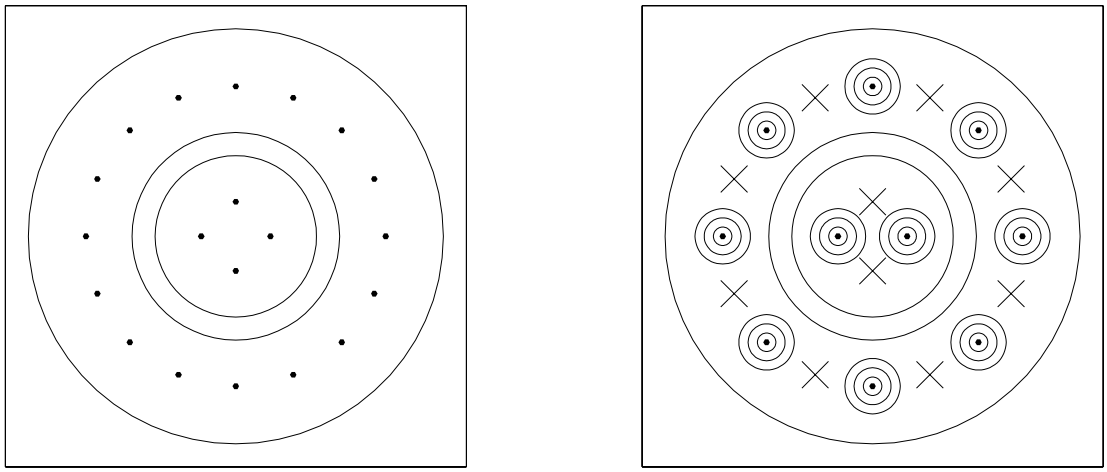

Figure 7: Fixed points of T^n_0 (left) become elliptic or hyperbolic points of T^n_ϵ (right).

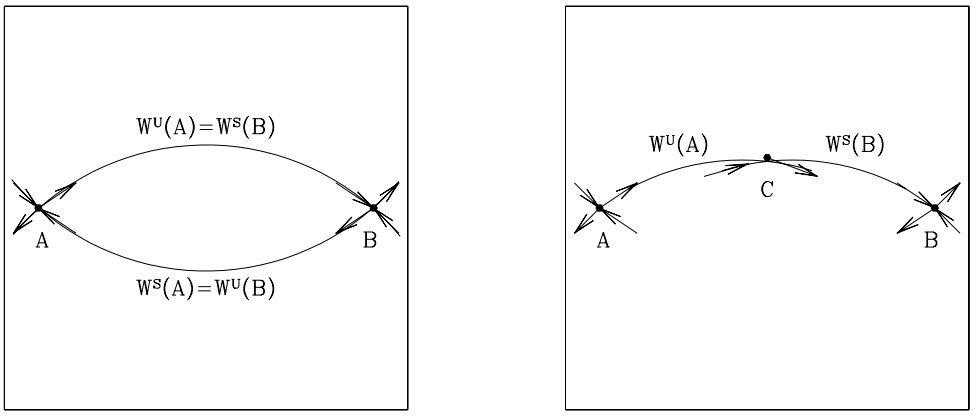

Figure 8: Left: heteroclinic connection in an integrable Hamiltonian system. The stable manifold of point A and the unstable manifold of point B are identical. Right: in a non-integrable Hamiltonian system, stable and unstable manifolds cross transversely.

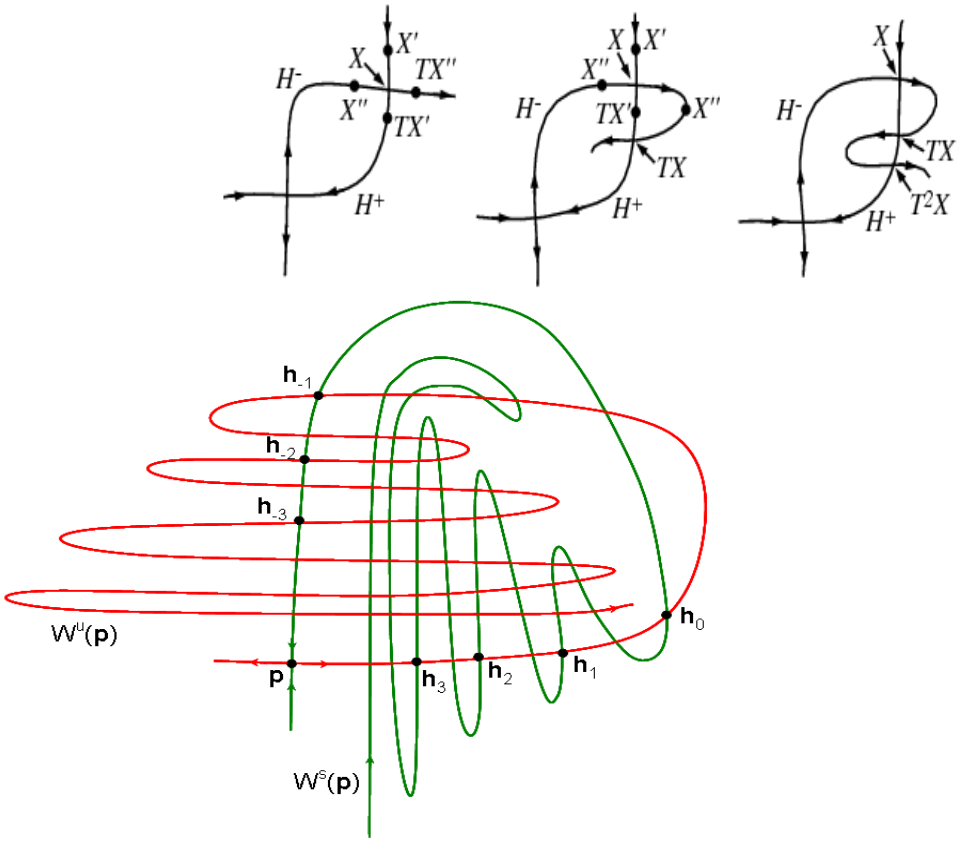

Figure 9: Homoclinic tangles. Above: From E. Weisstein, *Homoclinic Tangle*, MathWorld: A Wolfram Web Resource. http://mathworld.wolfram.com/HomoclinicTangle.html
Below: From P. So, *Unstable periodic orbits*, Scholarpedia 2(2): 1353

Figure 10: Non-integrable perturbation of integrable Hamiltonian system. Solid ellipses: some tori survive (those whose winding numbers are sufficiently far from any rational with small denominator). Others break into alternating elliptic and hyperbolic points. Around each elliptic point is a set of elliptical trajectories. Each hyperbolic point is surrounded by a chaotic region. From V.I. Arnol'd, *Small denominators and problems of stability of motion in classical and celestian mechanics*, Russian Mathematical Surveys **18:6**, 85–191 (1963). Russian version: Uspekhi Matematischeskikh Nauk. Reprinted in *Hamiltonian Dynamical Systems: a reprint collection*, ed. R.S. MacKay & J.D. Meiss, Adam-Hilger, 1987.

5 KAM Theorem

We have seen from the Poincaré-Birkhoff Theorem that tori with rational winding numbers are destroyed when a non-integrable perturbation is introduced. What about tori with irrational winding numbers? It turns out that, if the perturbation is sufficiently small, some such tori survive.

The size of the perturbation necessary to destroy a torus depends on the winding number of the torus. A torus whose winding number is close to a rational with small denominator, (i.e. is "not very irrational") will be destroyed by a small perturbation. A torus whose winding number is sufficiently far from all rationals with small denominators (i.e. is "very irrational") will require a large perturbation to be destroyed. The "most irrational" number, as we have seen in a previous chapter, is the golden mean $(1+\sqrt{5})/2$. The corresponding torus is the last to be destroyed, i.e. the perturbation required is the largest.

The KAM theorem was
– stated by **Kolmogorov** in 1954
– proved by **Arnold** in 1961-3
– generalized by **Moser** in 1962.

The KAM theorem states:
$\exists K(\epsilon)$ such that

$$\lim_{\epsilon\to 0} K(\epsilon) = 0 \tag{27}$$

and such that if $\forall m, n$,

$$\left| w - \frac{m}{n} \right| > \frac{K(\epsilon)}{n^{5/2}} \tag{28}$$

then the torus with winding number w survives a perturbation of size ϵ.

We can estimate the measure of the interval of winding numbers corresponding to surviving tori. Each denominator n corresponds to roughly n rationals $0, 1/n, 2/n, \ldots (n-1)/n$. Surrounding each rational is an interval of width $2K/n^{5/2}$ of w values which are the winding number values of possibly destroyed tori. We take the sum

$$\sum_{n=1}^{\infty} \frac{2K(\epsilon)}{n^{5/2}} n = 2K(\epsilon) \sum_{n=1}^{\infty} \frac{1}{n^{3/2}} \leq 2K \int_{n=1}^{\infty} dx \frac{1}{x^{3/2}} = 2K(\epsilon) \left[-\frac{2}{3} \frac{1}{x^{1/2}} \right]_1^{\infty} = \frac{4K(\epsilon)}{3} \tag{29}$$

Since $\lim_{\epsilon\to 0} K(\epsilon) = 0$, we have $4K(\epsilon)/3 < 1$ for ϵ sufficiently close to zero, and, for these values, the set of winding numbers of surviving tori has finite (non-zero) measure.

6 Three-body problem

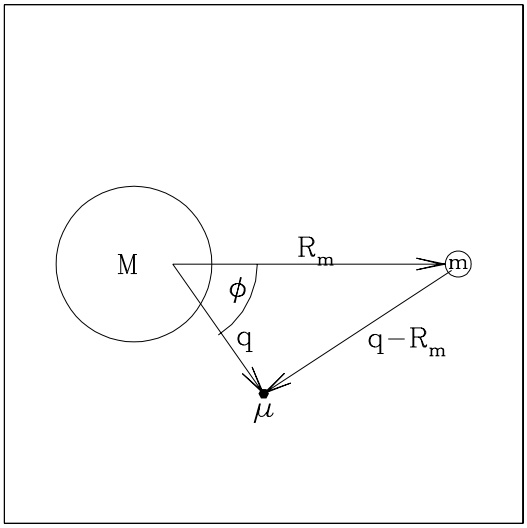

Figure 11: Configuration of the circular restricted three-body problem. Mass m has a circular orbit around mass M. Neither is affected by mass μ.

One of the main motivations for studying the mechanics of celestial systems has been to determine whether the solar system is stable. Even the three-body problem, however, is known to be non-integrable. Here we discuss the **circular restricted three-body problem (CRTBP)**, studied by Euler, Lagrange, Jacobi, Hill, Poincaré, Levi-Civita and Birkhoff.

We assume three bodies of varying masses:

$$M \gg m \gg \mu \tag{30}$$

The smallest body (like a moon or an asteroid) of mass μ moves under the influence of the largest body (like a sun) of mass M, and of the intermediate body (like a planet) of mass m. The two-body problem describing the interaction between M and μ is integrable. The additional intermediate body m introduces a non-integrable perturbation to the system.

The assumption (30) is used to:
–neglect the effect of the body of mass μ on the other two, and to
–identify the center of mass of the $M - m$ system with the center of M.
In addition, we assume that:
–m rotates about M in a circular orbit, and
–μ remains in the plane containing M and m.

We write the Hamiltonian governing the motion of mass μ, located at position $\mathbf{q}$. Mass μ is a distance $|\mathbf{q}|$ from mass M, a distance $|\mathbf{q} - \mathbf{R}_m|$ from mass m and has momentum $\mathbf{p}$.
We sum the kinetic energy and the gravitational potential energies resulting from the attraction to mass

M and to mass m to obtain the Hamiltonian:

$$\mathcal{H}(\mathbf{q},\mathbf{p},t) = \frac{|\mathbf{p}|^2}{2\mu} - \frac{GM\mu}{|\mathbf{q}|} - \frac{Gm\mu}{|\mathbf{q}-\mathbf{R}_m(t)|} \tag{31}$$

We begin by analyzing the two-body $M-\mu$ Hamiltonian:

$$\mathcal{H}_0(\mathbf{q},\mathbf{p}) = \frac{|\mathbf{p}|^2}{2\mu} - \frac{GM\mu}{|\mathbf{q}|} \tag{32}$$

The position $\mathbf{q}$ of mass μ is described by polar coordinates (r,ϕ), while its momentum $\mathbf{p}$ is described by (p_r, p_ϕ), where $p_r = \mu\dot{r}$ and $p_\phi = \mu r^2\dot{\phi}$ is the conserved angular momentum, leading us to rewrite $\mathcal{H}_0$ as:

$$\mathcal{H}_0(\mathbf{q},\mathbf{p}) = \frac{p_r^2 + p_\phi^2/r^2}{2\mu} - \frac{GM\mu}{r} \tag{33}$$

$$\frac{dr}{dt} = \frac{\partial\mathcal{H}_0}{\partial p_r} = \frac{p_r}{\mu} \qquad \frac{dp_r}{dt} = -\frac{\partial\mathcal{H}_0}{\partial r} = \frac{p_\phi^2}{\mu r^3} - \frac{GM\mu}{r^2} \tag{34a}$$

$$\frac{d\phi}{dt} = \frac{\partial\mathcal{H}_0}{\partial p_\phi} = \frac{p_\phi}{\mu r^2} \qquad \frac{dp_\phi}{dt} = -\frac{\partial\mathcal{H}_0}{\partial \phi} = 0 \tag{34b}$$

Mass m follows a circular orbit and so $\mathbf{R}_m(t)$ is not constant, since it changes orientation. In this case, we wish our perturbed Hamiltonian system to have $N=2$ degrees of freedom (r,ϕ,p_r,p_ϕ) but to be autonomous, i.e. not explicitly dependent on time. We therefore go into a rotating frame, defining:

$$\phi' = \phi - \Omega t \tag{35a}$$

$$\frac{d\phi'}{dt} = \frac{d\phi}{dt} - \Omega \tag{35b}$$

$$\frac{\partial\mathcal{H}'}{\partial p_\phi} = \frac{d\phi'}{dt} = \frac{p_\phi}{\mu r^2} - \Omega \tag{35c}$$

Although ϕ has been replaced by the new angle ϕ', the momentum p_ϕ has not been redefined. Using (35c) and $\mathbf{q}' = (r,\phi')$, we have

$$\mathcal{H}_0'(\mathbf{q}',\mathbf{p}) = \frac{p_r^2 + p_\phi^2/r^2}{2\mu} - \Omega p_\phi - \frac{GM\mu}{r} \tag{36}$$

$$\mathcal{H}'(\mathbf{q}',\mathbf{p}) = \frac{p_r^2 + p_\phi^2/r^2}{2\mu} - \Omega p_\phi - \frac{GM\mu}{r} - \frac{Gm\mu}{|\mathbf{q}'-\mathbf{R}_m|} \tag{37}$$

where $\mathbf{R}_m$ is now constant. Now $\mathcal{H}'$ depends on $(\mathbf{q}',\mathbf{p})$ but not on t. We now drop the primes in (36)-(37). Since $\mathcal{H}_0$ is independent of both t and ϕ, both $\mathcal{H}_0$ and p_ϕ are conserved and so $\mathcal{H}_0$ is integrable. ($\mathcal{H}$, however, does depend on ϕ through $\mathbf{q}'$.) One action variable, I_ϕ, for $\mathcal{H}_0$ is merely p_ϕ:

$$I_\phi = \frac{1}{2\pi}\oint_0^{2\pi} p_\phi\, d\phi = p_\phi \tag{38}$$

while the action variable I_r for $\mathcal{H}_0$ is computed as

$$p_r^2 = 2\mu(H_0 + \Omega I_\phi + GM\mu/r) - I_\phi^2/r^2 \tag{39}$$

$$I_r = \frac{1}{2\pi}\oint p_r dr = -I_\phi + \frac{GM\mu^2}{\sqrt{-2\mu(H_0+\Omega I_\phi)}} \tag{40}$$

$$
\begin{aligned}
I_r &= -I_\phi + \frac{GM\mu^2}{\sqrt{-2\mu(H_0+\Omega I_\phi)}} \\
\frac{\sqrt{-2\mu(H_0+\Omega I_\phi)}}{GM\mu^2} &= \frac{1}{I_r+I_\phi} \\
H_0 &= -\Omega I_\phi - \frac{1}{2\mu}\left(\frac{GM\mu^2}{I_r+I_\phi}\right)^2 \equiv \mathcal{H}_0(I_r, I_\phi)
\end{aligned} \tag{41}
$$

The Hamiltonian (41) leads to the frequencies

$$\omega_{0r} = \frac{\partial H_0}{\partial I_r} = \frac{(GM)^2\mu^3}{(I_r+I_\phi)^3} \equiv \omega_\mu \tag{42a}$$

$$\omega_{0\phi} = \frac{\partial H_0}{\partial I_\phi} = -\Omega + \frac{(GM)^2\mu^3}{(I_r+I_\phi)^3} = -\Omega + \omega_\mu \tag{42b}$$

The frequency ω_μ is the frequency of body μ in the non-rotating reference frame. The ratio between the two frequencies is

$$\frac{\omega_{0\phi}}{\omega_{0r}} = \frac{-\Omega+\omega_\mu}{\omega_\mu} = 1 - \frac{\Omega}{\omega_\mu} \tag{43}$$

The ratio (43) is the winding number relevant to the Poincaré-Birkhoff and KAM theorems. For the case when M is the sun and m is the planet Jupiter, the breakup of tori with rational winding numbers predicted by the Poincaré-Birkhoff theorem leads to the **Kirkwood gaps** in the frequencies (or orbital paths) of asteroids μ. For the case in which M is the planet Saturn, m is one of the moons of Saturn, the theorem leads to gaps in the particles μ in the rings of Saturn.

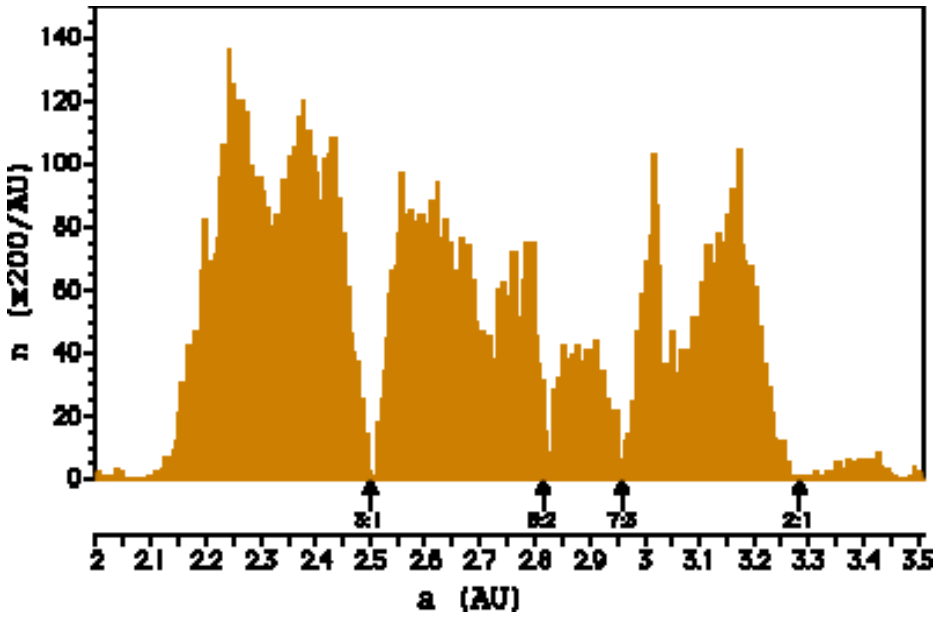

Figure 12: Gaps in the distribution of main belt asteroids with orbital period (or equivalently, semi-major axis in astronomial units AU). They correspond to the location of orbital resonances with Jupiter. From Wikepedia, *Kirkwood gap.*

7 Billiards

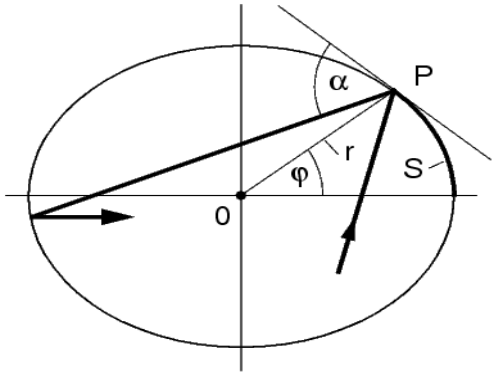

Figure 13: Generalized billiard table $r(\phi)$ and trajectory. Each bounce is described by its angular position ϕ and its angle α with the tangent to the table. From H.J. Korsch & F. Zimmer, *Chaotic Billiards*, `http://kluedo.ub.uni-kl.de/frontdoor.php?source_opus=1202`.

Billiards reveal a great deal about Hamiltonian dynamics. See, for example L. Bunimovich, *Dynamical billiards*, Scholarpedia 2(8):1813, *Dynamical billiards* in Wikipedia, or E. Weisstein, *Billiards* in Mathworld. Our treatment is taken from H.J. Korsch & J.-J. Jodl, *Chaos* (Springer, 1994, 1998) and from H.J. Korsch & F. Zimmer, *Chaotic Billiards*, Fachbereich Physik, Univ. Kaiserslautern `http://kluedo.ub.uni-kl.de/frontdoor.php?source_opus=1202`. See also M.V. Berry, *Regularity and chaos in classical mechanics, illustrated by three deformations of a circular billiard*, Eur. J. Phys **2**, 91-102 (1981) and `http://www.phy.bris.ac.uk/people/Berry_mv/the_papers/Berry102.pdf`

We consider billiards in a domain bounded by a closed curve parametrized by an angle ϕ

$$r = r(\phi) \tag{44}$$

(One can also introduce obstacles in the interior of the domain, off which the billiard bounces.) Each impact is described by two scalars, as shown in figure 13. The first, a kind of position, is ϕ. The second, a kind of velocity, is the angle α between the exiting trajectory and the tangent to the boundary $r(\phi)$. The mapping takes one bounce to the next:

$$(\phi_n, \alpha_n) \Longrightarrow (\phi_{n+1}, \alpha_{n+1}) \tag{45}$$

Alternately, the location can be given by the arclength S along the table and/or the angle described by $p = \cos(\alpha)$ so that

$$(S_n, p_n) \Longrightarrow (S_{n+1}, p_{n+1}) \tag{46}$$

Many kinds of curves have been considered. The **circle** $r = c$ always gives rise to integrable dynamics since the angle α is constant. The orbits are periodic if α is a rational fraction of 2π and quasiperiodic if α is an irrational fraction of 2π. It turns out that **elliptical billiards**, trajectories in which are shown in figure 14, are also integrable. The **stadium**, studied by Bunimovich, consists of a pair of line segments connected by two semi-circles. The dynamics in stadium billiards is **ergodic**: all points are visited. We therefore consider **cosine billiards**

$$r(\phi) = 1 + \epsilon \, \cos(\phi) \tag{47}$$

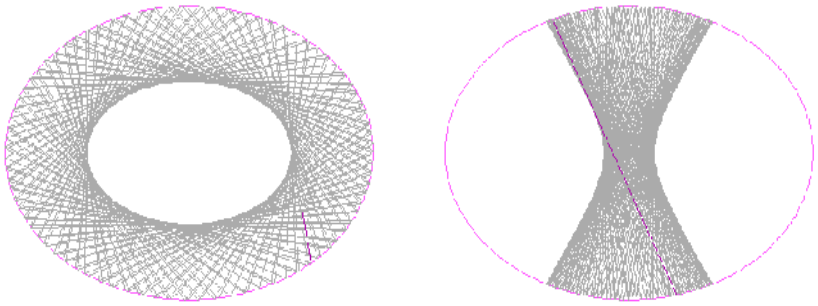

Figure 14: Two types of trajectories in an elliptical billiard. From H.J. Korsch & F. Zimmer, *Chaotic Billiards*, `http://kluedo.ub.uni-kl.de/frontdoor.php?source_opus=1202`.

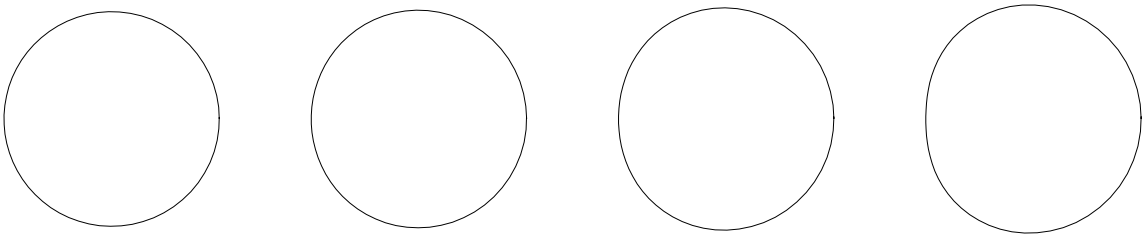

Figure 15: Shape of cosine billiard table for $\epsilon = 0.1$, 0.2, 0.3, 0.4.

a table whose shape is shown in figure 15.

For $\epsilon = 0$, we have the integrable circle case. All points belong to simple orbits, periodic or quasiperiodic. Figure 16 shows trajectories in the (S, p) phase plane. As ϵ increases, we can see the tori break up, beginning with those whose winding numbers are fractions with small denominators.

The table below gives the low-denominator fractions m/n and the corresponding angles α. These are the first tori to be destroyed. In contrast, the most long-lived torus (i.e. which survives the highest ϵ). has as its winding number the golden mean w^*.

m/n	α	$p = \cos(\alpha)$	m/n	α	$p = \cos(\alpha)$
$1/2$	$90°$	0	$1/5$	$36°$	0.809
$1/3$	$60°$	$1/2$	$2/5$	$72°$	0.309
$2/3$	$120°$	$-1/2$	$3/5$	$108°$	-0.309
$1/4$	$45°$	$1/\sqrt{2}$	$4/5$	$144°$	-0.809
$3/4$	$135°$	$-1/\sqrt{2}$			
$\sqrt{2}$	$127.279°$	-0.6057	$w^* = 0.618$	$291.262°$	0.3626

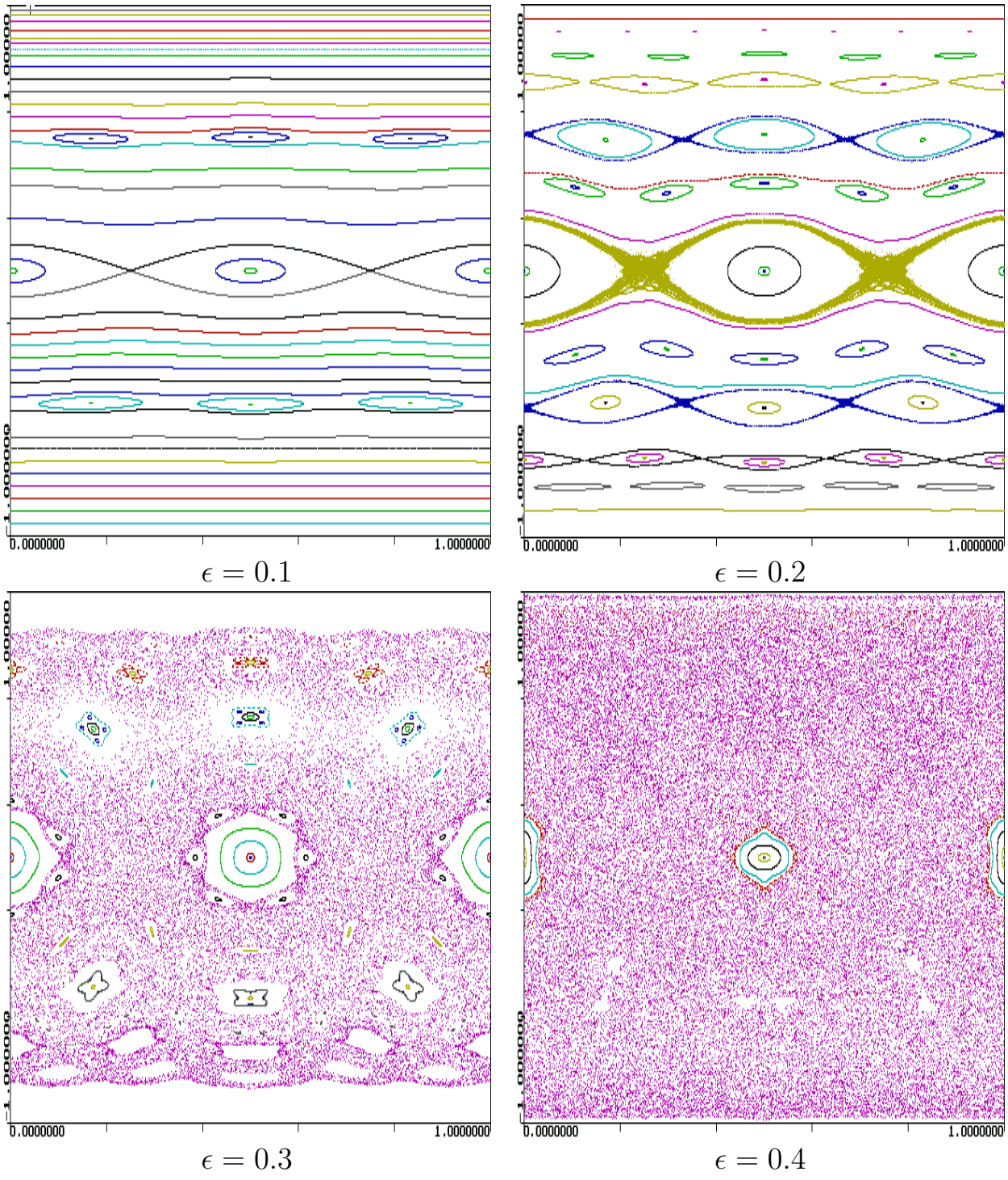

Figure 16: Phase plane for cosine billiard $r = 1+\epsilon\cos\phi$ as ϵ increases from 0.1 to 0.4. Horizontal axis is S, the arclength along the table at which the bounce occurs. Vertical axis is $p = \cos(\alpha)$, with α the angle between the exiting trajectory and the tangent to the table. For $\epsilon = 0.1$ (top left), there are still many periodic and quasiperiodic trajectories. These are destroyed as ϵ is increased. From H.J. Korsch & F. Zimmer, *Chaotic Billiards*, `http://kluedo.ub.uni-kl.de/frontdoor.php?source_opus=1202`.

8 Fluid dynamics

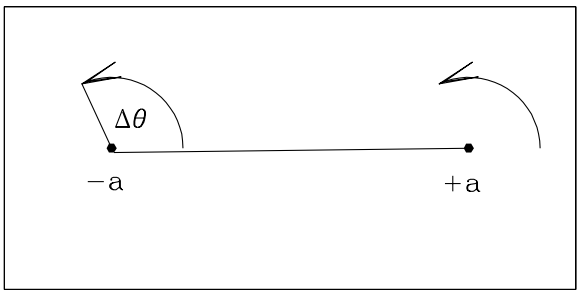

Figure 17: Configuration of the blinking vortex. The vortex on the right is switched on for a time T, causing rotation of the surrounding fluid by an angle $\Delta\theta$. Then the vortex on the left is switched on.

As stated in section 1, the fluid-dynamical streamfunction can play the role of a Hamiltonian:

$$\frac{dx}{dt} = u = -\frac{\partial\psi}{\partial y} \qquad\qquad \frac{dy}{dt} = v = \frac{\partial\psi}{\partial x} \tag{48}$$

The modern study of kinematical fluid mechanics as a Hamiltonian system was initiated by H. Aref, *Stirring by chaotic advection*, J. Fluid Mech. **143**, 1–21 (1984). In this context, chaos can be desirable since it promotes rapid mixing.

As stated in section 3, the simplest non-integrable Hamiltonian system has one degree of freedom (two variables), like (48) and temporal periodic forcing. In **blinking vortex system** of Aref, two vortices located at $\pm a$ both with strength κ are alternately switched on and off, each for a time T. In the absence of solid boundaries, vortex A causes the fluid at (x, y) to rotate around $(+a, 0)$ to (x', y') via

$$\begin{pmatrix} x' \\ y' \end{pmatrix} = \begin{pmatrix} a \\ 0 \end{pmatrix} + \begin{pmatrix} \cos\Delta\theta & -\sin\Delta\theta \\ \sin\Delta\theta & \cos\Delta\theta \end{pmatrix} \begin{pmatrix} x-a \\ y \end{pmatrix} \tag{49a}$$

where $\Delta\theta_+(x, y) = \kappa T/((x-a)^2 + y^2)$ and then vortex B rotates the fluid around $(-a, 0)$ via

$$\begin{pmatrix} x'' \\ y'' \end{pmatrix} = \begin{pmatrix} -a \\ 0 \end{pmatrix} + \begin{pmatrix} \cos\Delta\theta & -\sin\Delta\theta \\ \sin\Delta\theta & \cos\Delta\theta \end{pmatrix} \begin{pmatrix} x'+a \\ y' \end{pmatrix} \tag{49b}$$

where $\Delta\theta_-(x', y') = \kappa T/((x'+a)^2 + y'^2)$. This configuration is shown in figure 17. The non-dimensional parameter

$$\mu = \kappa T/a^2 \tag{50}$$

controls the degree of non-integrability, as shown in figure 18.

Flows such as the blinking vortex were realized experimentally by J.M. Ottino, whose book, *The kinematics of mixing: stretching, chaos and transport* (Cambridge Univ. Press, 1989) is devoted to this subject.

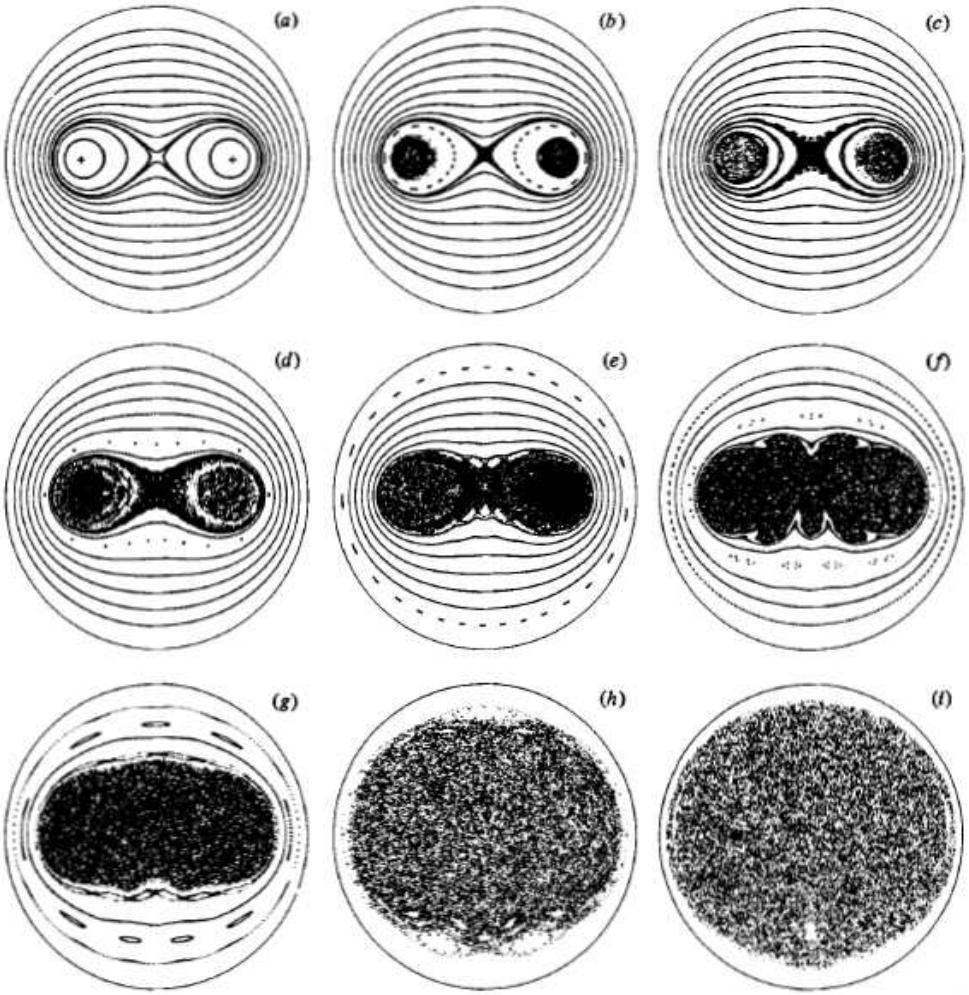

FIGURE 2. Iterated-map results described in §4. Parameters are $\beta = 0.5$ and (*a*) $\mu = 0.05$; (*b*) 0.10; (*c*) 0.125; (*d*) 0.15; (*e*) 0.20; (*f*) 0.35; (*g*) 0.50; (*h*) 1.0; (*i*) 1.5. Crosses indicate agitator positions.

Figure 18: Simulation of blinking vortex flow shows increasing degree of chaos as μ increases. From H. Aref, *Stirring by chaotic advection*, J. Fluid Mech. **143**, 1–21 (1984).

9 Bifurcations in Hamiltonian systems

Having seen the crucial role played in Hamiltonian systems (and thus in spatial analysis) by centers (elliptic fixed points) and saddles (hyperbolic fixed points), we now examine bifurcations of these points.

9.1 Hamiltonian saddle-node bifurcation

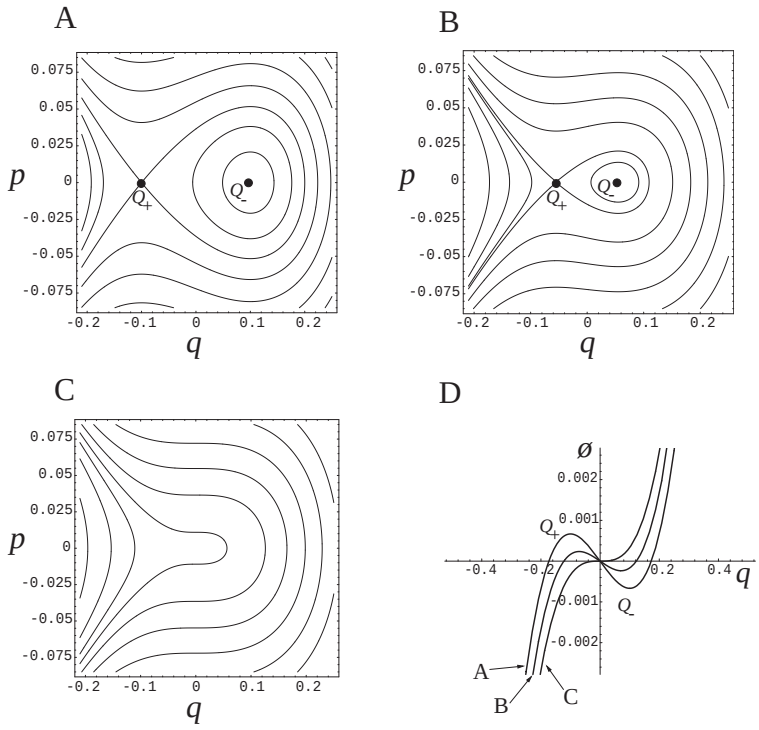

Figure 19: Phase portraits of the Hamiltonian saddle-node normal form (51), with $p = \dot{q}$. A: $\delta = 0.2$, B: $\delta = 0.1$, C: $\delta = 0$. D: Corresponding potential Φ associated to each phase portrait A, B or C, with $\dot{p} = -\partial\Phi/\partial q$. An elliptic region bounded by the separatrix that starts and ends on the fixed point Q_+ (homoclinic orbit) is present on A and B. Phase portrait C displays the critical merging of fixed points Q_+ and Q_+, and the disappearance of the elliptic region.

The normal form for the Hamiltonian saddle-node bifurcation is

$$\ddot{q} = \delta - q^2 \Longleftrightarrow \left\{ \begin{array}{l} \dot{q} = p = \frac{\partial \mathcal{H}}{\partial p} \\ \dot{p} = \delta - q^2 = -\frac{\partial \mathcal{H}}{\partial q} \end{array} \right. \tag{51}$$

where

$$\mathcal{H} = \frac{p^2}{2} + \Phi(q) = \frac{p^2}{2} + \frac{q^3}{3} - \delta q \tag{52}$$

Figure 19D shows the potential Φ for various values of δ. The fixed points are extrema of Φ:

$$p = 0 \tag{53a}$$

$$q = \pm\sqrt{\delta} \text{ for } \delta > 0 \tag{53b}$$

Their stability is determined by the eigenvalues of

$$\begin{bmatrix} 0 & 1 \\ -2q & 0 \end{bmatrix} \Longleftrightarrow \lambda^2 = -2q \tag{54}$$

We have

$$q = +\sqrt{\delta} \Longleftrightarrow \lambda^2 < 0 \Longleftrightarrow \lambda \text{ imaginary } \Longleftrightarrow q \text{ a center} \tag{55a}$$

$$q = -\sqrt{\delta} \Longleftrightarrow \lambda^2 > 0 \Longleftrightarrow \lambda \text{ real } \Longleftrightarrow q \text{ a saddle} \tag{55b}$$

So at $\delta = 0$, a saddle and center are created simultaneously, as is shown in figure 19A,B,C.

9.2 Hamiltonian pitchfork bifurcation

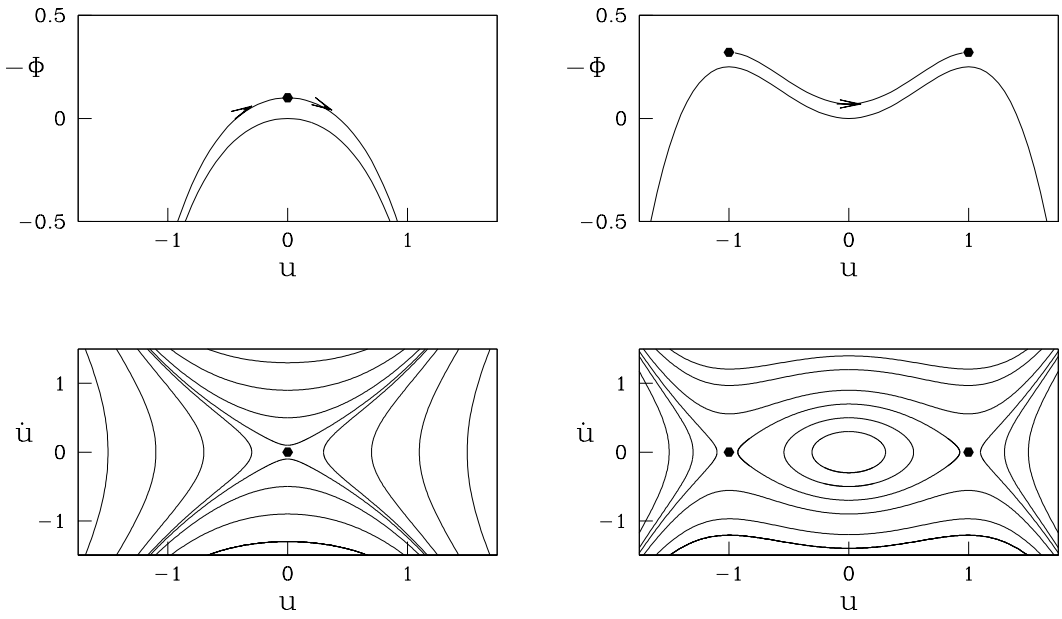

Figure 20: Behavior of the Ginzburg-Landau equation for $\mu = -1$ and for $\mu = +1$.
Top row: potential $-\Phi(u)$ with fixed points $\bar{u} = 0$ for $\mu = -1$ and $\bar{u} = \pm\sqrt{\mu} = \pm 1$ for $\mu = +1$. For $\mu = -1$, a portion of a trajectory is shown which originates at $u = -\infty$ and goes to $u = +\infty$. For $\mu = +1$, the trajectory shown goes from $\bar{u} = -1$ to $\bar{u} = +1$.
Bottom row: phase portraits in the $(u, \dot{u})$ plane. $(0, 0)$ is a hyperbolic fixed point for $\mu = -1$ and an elliptic fixed point for $\mu = +1$. $(\sqrt{\mu}, 0)$ are hyperbolic fixed points for $\mu = +1$ and are connected by a heteroclinic orbit.

In figure 20, already presented in a previous section, we show how a saddle is transformed into a center surrounded by two saddles. Defining

$$\mathcal{H} = \frac{v^2}{2} - \Phi(u) = \frac{v^2}{2} - \frac{u^4}{4} + \mu\frac{u^2}{2} \tag{56}$$

the equations of motion are:

$$\ddot{u} = u^3 - \mu u \Longleftrightarrow \begin{cases} \dot{u} = v = \partial\mathcal{H}/\partial v \\ \dot{v} = u^3 - \mu u = -\partial\mathcal{H}/\partial u \end{cases} \tag{57}$$